Journal of Alloys and Compounds 503 (2010) 213–219

Contents lists available at ScienceDirect

Journal of Alloys and Compounds

journal homepage: www.elsevier.com/locate/jallcom

Effect of illumination and frequency on the capacitance spectroscopy and the relaxation process of p-ZnTe/n-CdMnTe/GaAs magnetic diode for photocapacitance applications

G.B. Sakr, I.S. Yahia *

Physics Department, Faculty of Education, Ain Shams University, Roxy, Cairo, Egypt

ARTICLE INFO

Article history:
Received 10 February 2010
Received in revised form 29 April 2010
Accepted 29 April 2010
Available online 7 May 2010

Keywords:
P-ZnTe/n-CdMnTe/GaAs
Magnetic diode
Capacitance–frequency characteristics
Interface state
Relaxation time
Light sensitive capacitor

ABSTRACT

Heterostructure of p-ZnTe/n-CdMnTe/GaAs (II-VI/II-VI-DMS/III-V) is grown by molecular beam epitaxially growth (MBE). The capacitance–frequency (C–f) characteristics of the prepared heterostructure under dark and different illumination intensities were analyzed. The studied sample shows a capacitance illumination dependence. Modified Goswami and Goswami (G–G) model was used to interpret the capacitance profile under the effect of the irradiated light. The illumination dependence of the relative capacitance (C_{ph}/C_d) at different frequency was studied and interpreted. The interface density states (N_{ss}), the interface capacitance (C_{ss}) and dielectric relaxation time (τ) are increased with the increase of the illumination intensities. Therefore, the prepared heterostructure can be used as photocapacitance sensor in modern electronic and optoelectronic devices.

1. Introduction

Diluted magnetic semiconductors are compound of alloy semiconductor containing a large fraction of magnetic ions [1]. Currently, diluted magnetic semiconductors (DMSs) have been receiving large attention due to their potential for development of spintronic devices [2]. DMSs are expected to play an important role in interdisciplinary material science and electronics because charge and spin degrees of freedom accommodated into a single material exhibits interesting magnetic, magneto-optical, magneto-electronic and other properties [3].

The Mn-doped II-VI based semimagnetic semiconductors belong to an attractive materials owing to their unique properties and because of new possibilities of application in new modern devices [4]. Cadmium manganese telluride (CdMnTe) is one of the most studied semiconductor alloy, where a part of the Cd^{2+} ions is randomly replaced by Mn^{2+} ions having permanent magnetic moments. Without external magnetic fields, this DMS behaves in away similar to normal ternary semiconductors. CdMnTe has been a focus of interest for decades in a quantum well (QW) structures because of its potential application in spintronics and the abundance of novel physical phenomena [5]. DMS is a good candidate material for many practical applications, such as magnetic field sensors, solar cells, optical isolators, lasers, etc. Recently, an increased attention has been paid to CdMnTe because it is revealed that the material is a good candidate to compete with CdZnTe in X-ray and γ-ray nuclear detector applications [6]. Over the past decade, there has been an added interest in studying cadmium manganese telluride in connection with attempts to produce spintronics devices [7]. The above possibilities inherent in this material, make it a promising for much more applications.

With the progress of crystal growth techniques such as molecular beam epitaxy (MBE) it became possible to grow different semiconducting devices such as: quantum well, quantum dot, heterostructure, photovoltaic and solar cells, spintronic devices, etc. [5]. Heterostructure based on diluted magnetic semiconductor can be grown easily with MBE technique. Because of these advantages, there is a growing interest in the fabrication of this type of materials of p-ZnTe/ n-CdMnTe/GaAs (II-VI/II-VI-DMS/III-V) in optoelectronic devices employing (II-VI-DMS) as an active materials. This device represents a simple, low cost and versatile alternative to the new type of electronic and optoelectronic devices.

In the recent years, there has been an explosion in the use of capacitive sensing interfaces for human-input controls. From mobile handsets to computers, point-of-service terminals to home electronics and medical devices to industrial controls. Capacitive sensing is showing up in applications everywhere. Capacitive sensors can directly sense a variety of things; motion, chemical

* Corresponding author. Tel.: +20 182848753; fax: +20 22581243.
E-mail addresses: dr_isyahia@yahoo.com, isyahia@gmail.com (I.S. Yahia).

0925-8388/$ – see front matter © 2010 Elsevier B.V. All rights reserved.
doi:10.1016/j.jallcom.2010.04.235

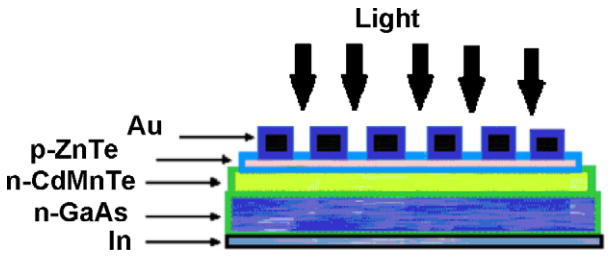

Fig. 1. Schematic diagram of the Au/p-ZnTe/n-CdMnTe/n-GaAs/In device.

composition, electric field and, indirectly, sense many other variables which can be converted into motion or dielectric constant such as: pressure, acceleration, fluid level, and fluid composition. They are built with conductive sensing electrodes in a dielectric, with excitation voltages on the order of five volts and detection circuits which turn a capacitance variation into a voltage, frequency, or pulse width variation. A number of different semiconductors systems have been used to make piezoresistive or capacitive sensors, including Si, SiC and diamond. The wide bandgap semiconductors are capable of operating at much higher temperature than Si, with SiC-based piezoresistive sensors demonstrated up to temperature of 600 °C [8–11].

In the present work, we prepared the heterostructure of p-ZnTe/n-CdMnTe/n-GaAs by MBE technique for light sensitive capacitor. Effect of illumination intensity on the capacitance profile of p-ZnTe/n-CdMnTe/GaAs was studied under different frequencies. Modified Goswami and Goswami (G–G) model was used for the first time to interpret the variation of the device capacitance. From the *C–f* measurements, values of the interface density states N_{ss}, the interface capacitance C_{ss} and relaxation time τ were extracted.

2. Experimental procedures

In the present work, the prepared heterostructure device was grown in the EPI-620 MBE system at the Institute of Physics, Polish Academy of Sciences, Poland. MBE system consisted of two main chambers: the first one is the load-lock ultra high vacuum (UHV) chamber (typical pressure 10^{-9} to 10^{-10} Torr), used for loading substrates without breaking the vacuum environment. The second one is the growth chamber with a typical pressure about 10^{-10} Torr inside it. Both of these chambers are connected via the UHV valve. The UHV inside the MBE system is achieved using cryo- and turbo molecular pumps connected directly to these chambers. In addition, one should notice that the growth chamber is cooled down with liquid nitrogen. The sources and the growth environment need to be surrounded by liquid nitrogen-cooled cryopanels to minimize unintentional impurity incorporation in the deposited layers from the residual background, while the whole system is confined within UHV environment. Molecular beams are being generated from six thermal elemental effusion cell sources of high purity materials: Cd, Te, Mn, Mg, Zn, and ZnI_2 (used for n-type doping) installed in the growth chamber. For p-type doping, a RF-plasma source of excited nitrogen plasma has been used.

High quality (1 0 0)-oriented semi-insulating or n^+ Si-doped GaAs crystals were used as a substrate. Prior to the growth process, the protective oxide layer has been removed from the substrate by thermal annealing. During the thermal treatment the surface of the GaAs substrate was controlled by reflection high-Energy electron diffraction (RHEED) technique. The sequence of the grown layers on GaAs substrate was as follows: (1) the first grown layer on n-GaAs was CdMnTe of thickness 3.338 μm as an active material (absorber) and (2) the second grown layer was ZnTe of thickness 0.424 μm as a window. The thickness of the ZnTe and CdMnTe layers were determined in situ by RHEED oscillations. Schematic diagram of the grown layers were shown in Fig. 1. The upper contact of the device has a mesh style made from thermally evaporated of Au using thermal evaporation system Edwards 306 A. The back contact of the GaAs crystal was directly fabricated by soldering a high pure indium. The total area of the device was $A = 0.4725\ cm^2$ and the effective area equals $0.216\ cm^2$.

The cell capacitance (C) and resistance (R) were measured directly at different frequencies using a programmable automatic RLC bridge (PM 6304 Philips&Fluke). All investigated samples are represented on the screen of the bridge by a resistance R connected in parallel with a capacitance C as an equivalent circuit in dark and illumination conditions. Special designed holder was used to connect both the lower and upper parts of the studied sample to the RLC bridge. The source of light was a high power tungsten filament lamp. The intensity of light was measured with a solar power meter (TM-206). The intensity of light was varied by changing the voltage across the tungsten lamp. It should be mentioned that all the measurements were carried out at room temperature in the air ambient.

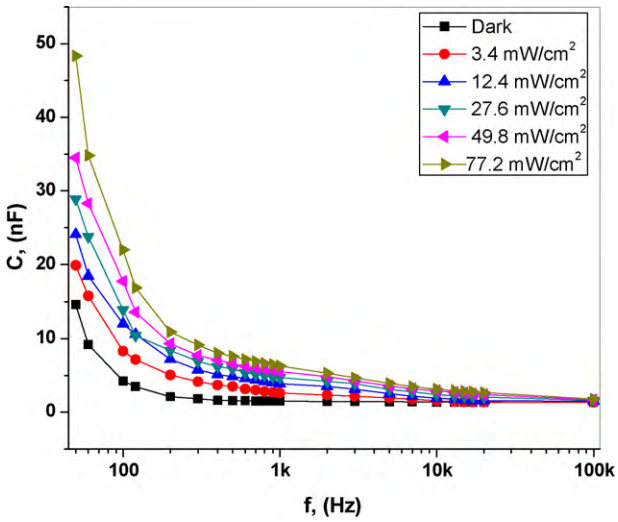

Fig. 2. Semi-logarithmic plot of the cell capacitance C versus the applied frequency f at different illumination intensities.

3. Results and discussion

The *C–f* measurements give an important information about the density or energy distribution of the interface states of the prepared device. The technique is based on the strong dependence of semiconducting junction admittance on ac signal frequency and temperature and in the case of a semiconductor with an incompletely ionized impurity. In general, the *C–f* plots in the idealized case are frequency independent [12–15]. However, this idealized case is often disturbed due to the presence of the interface states at the interfacial layer and with the semiconductor interface [16–19]. At low ac signal, the charge is exchanged between the interface states and the semiconductor and so, the measured junction capacitance is the sum of the space charge and interface states capacitance [20].

Fig. 2 shows the capacitance–frequency dependence at different illumination intensities. At low frequencies, the variation of capacitance with frequency is stronger than at the higher frequencies, which indicates the presence of interface states at the junction. The higher values of capacitance at low frequencies are due to excess capacitance resulting from the interface states in equilibrium with the n-GaAs that can follow the ac signal. The decrease of the capacitance values in the intermediate frequency region means that small part of the interface states can only follow the signal [21,22]. Fig. 3 illustrates the illumination dependence of the capacitance at different frequencies. It is clear from this figure that the capacitance has both a strong illumination and frequency dependencies. The values of the capacitance depend on a number of parameters such as the thickness, series resistance and density of interface states. With the increase of the illumination intensities, concentration of charge carriers increases logarithmically. Therefore, the polarizability due to the charge transfer of charge carriers as electrons and holes [23], the interfacial polarization and the density of interface states also increases. The increase of the charge carrier concentration under illumination leads to an improvement of the space charge layer [24]. It is interesting to note that after irradiation of the prepared heterostructure device with light, a considerable increase of the junction capacitance because of the increase of the number of radiation induced deep defects in the material [25]. Due to thermal annealing [26] and/or illumination with light [27],

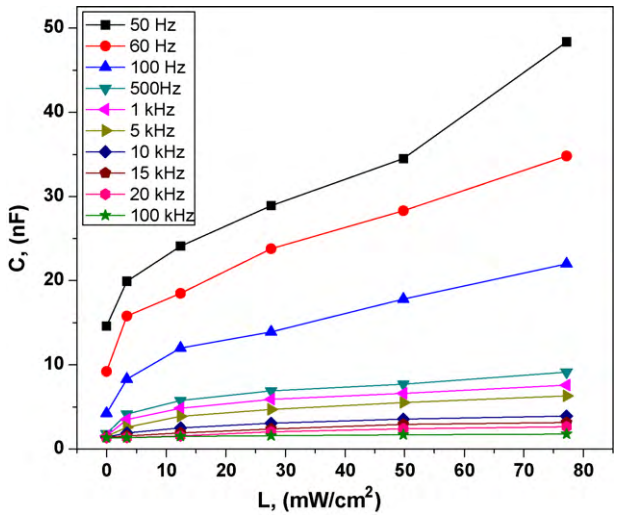

Fig. 3. The illumination dependence of the cell capacitance C at different frequency.

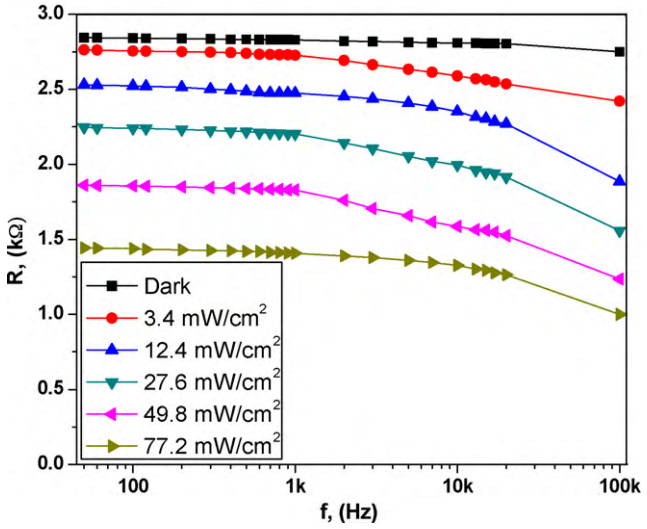

Fig. 4. Semi-logarithmic plot of the cell resistance R versus the applied frequency f at different illumination intensities.

these defects heal out restoring to a large extend the initial device performance.

The decrease of C with frequency can be attributed to the fact that at low frequencies, the cell capacitance C for polar materials is due to the contribution of multicomponent of polarization, deformational polarization (electronic and ionic) and relaxation polarization (orientation and interfacial). When the frequency increased, the dipoles cannot be able to rotate sufficiently rapidly, so that their oscillations lag behind those of the field. As the frequency is further increased, the dipole will be completely unable to follow the ac field and the orientation polarization stopped, so the capacitance C decreases approaching a constant value at the higher frequencies due to the interfacial polarization only, which is effective in multilayers structure [28].

In the previous work, Goswami and Goswami (G–G) model [29] was applied to interpret the capacitance profile under ac field according to the effect of temperature. In our work, we try to interpret the capacitance profile of the heterostructure junction under the effect of irradiated light as a modified Goswami and Goswami (G–G) model. The drastic increase of capacitance at the low frequency range is probably due to space charge polarization induced by the increasing number of free carriers generated due to the effect of different illumination intensities. The observed increase of capacitance with illumination may be qualitatively explained by the equivalent circuit model developed by G–G model of bulk resistance r_s in series with parallel R–C. According to this model, the measured capacitance C is given by [29]:

$$C = C_\infty + \frac{1}{\omega^2 R^2 C_\infty}, \tag{1}$$

where R is the cell resistance of the heterostructure, $\omega = 2\pi f$ is the angular frequency, C_∞ is the capacitance at the higher frequency and f is the applied frequency. According to the above equation, the increase of capacitance C with illumination may be due to the decrease of the value of R with illumination as shown in Fig. 4. The decrease in cell resistance with illumination is due to the increase of the free carriers with the effect of illumination. Accordingly, this can be explained by the enhancement of the photoconductivity of the p-ZnTe/n-CdMnTe/GaAs structure. It is clear from Eq. (1) that the decrease of R under the effect of illumination leads to the increase of the capacitance C. Furthermore, Eq. (1) also predicts that the measured capacitance should decreased with increasing the applied frequency reaching the constant (equilibrium) value of the capacitance at the higher frequency C_∞ [30–32] as illustrated in Fig. 1. This behavior can be attributed to the effect of charge redistribution by carrier hopping on defects [33–35]. At the lower frequency, the charge on the defects can be rapidly redistributed, so that defects closer to the positive side of the applied field become negatively charged, while defects closer to the negative side of the applied field become positively charged. This leads to a screening of the field and an overall reduction in the electrical field because capacitance is inversely proportional to the field [36] and this leads to the increase of the capacitance. At the higher frequency, the defects no longer have enough time to rearrange inversions to the applied voltage; hence, the capacitance decreases to the minimum value C_∞. It is observed that the high illumination intensity is more effective on the carrier hopping because of the number of free carriers increased.

It is known that, the capacitance depends on the polarizability of the material [37–42] and there are several sources of polarizability: (1) dipolar α_{dip}, (2) ionic polarization α_i, (3) electronic α_e, and (4) interfacial or space charge polarization α_{int}. Thus, the total polarizability of the material at dark conditions α_d may be written as [23]:

$$\alpha_d = \alpha_{dip} + \alpha_e + \alpha_i + \alpha_{\text{int}}, \tag{2}$$

The total polarizability α_T of sample under illumination is given by:

$$\alpha_T = \alpha_{dip} + \alpha_e + \alpha_i + \alpha_{\text{int}} + \alpha_{ph}, \tag{3}$$

where α_{ph} is the polarizability under illumination due to the transfer of electron/holes charge carriers. Total polarizability α_T and the concentration of charge carriers are highly dependent on illumination intensities. In general form, the relationship between the relative dielectric constant, charge carrier concentration and polarizability of the molecule is determined by Clausius–Mosotti relation [39]:

$$\frac{\varepsilon_d - 1}{\varepsilon_d + 2} = \frac{N_d \alpha_d}{3\varepsilon_o} \tag{4}$$

where ε_d is the relative permittivity or dielectric constant in dark, ε_o is the permittivity of free space and N_d is the concentration of charge carriers in dark. From the above relation, the relative permittivity ε_d can be written as:

$$\varepsilon_d = \frac{3\varepsilon_o + 2N_d\alpha_d}{3\varepsilon_o - N_d\alpha_d}, \tag{5}$$

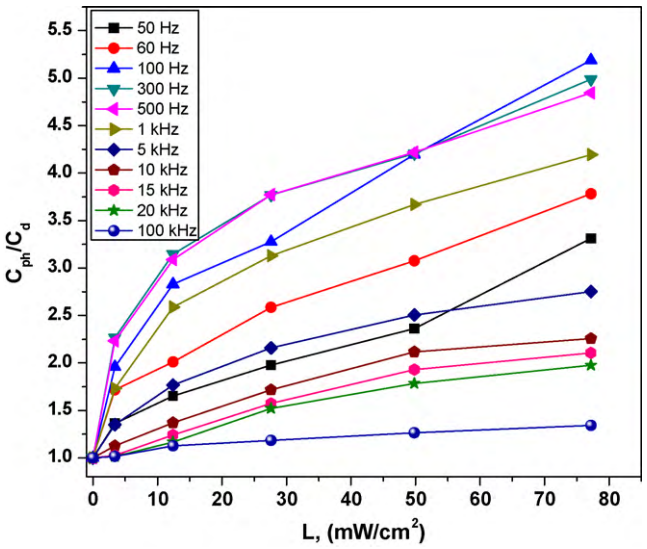

Fig. 5. Relative capacitance C_{ph}/C_d versus illumination intensities at different frequency.

Similar expression can be written for the dielectric constant under illumination ε_{ph} as follows:

$$\varepsilon_{ph} = \frac{3\varepsilon_o + 2N\alpha}{3\varepsilon_o - N\alpha}, \tag{6}$$

The value of $N\alpha$ depends upon illumination. The equation for $N\alpha$ can be written as:

$$N\alpha = N_d\alpha_d[1 + \log(1 + kL)], \tag{7}$$

where k is photocapacitive factor, L is the intensity of light. By substitution using the value of $N\alpha$ in Eq. (6), the dielectric constant under illumination ε_{ph} can be rewritten as:

$$\varepsilon_{ph} = \frac{3\varepsilon_o + 2N_d\alpha_d[1 + \log(1 + kL)]}{3\varepsilon_o - N_d\alpha_d[1 + \log(1 + kL)]}, \tag{8}$$

From Eqs. (5) and (8), we can derive the expression:

$$\frac{\varepsilon_{ph}}{\varepsilon_d} = \left(\frac{3\varepsilon_o + 2N_d\alpha_d[1 + \log(1 + kL)]/3\varepsilon_o - N_d\alpha_d[1 + \log(1 + kL)]}{3\varepsilon_o + 2N_d\alpha_d/3\varepsilon_o - N_d\alpha_d}\right), \tag{9}$$

At the lower illumination intensity, it can be considered that:

$$3\varepsilon_o - N_d\alpha_d[1 + \log(1 + kL)] = 3\varepsilon_o - N_d\alpha_d, \tag{10}$$

Now Eq. (9) can be written as:

$$\frac{\varepsilon_{ph}}{\varepsilon_d} = \left(\frac{3\varepsilon_o + 2N_d\alpha_d[1 + \log(1 + kL)]}{3\varepsilon_o + 2N_d\alpha_d}\right), \tag{11}$$

The relation between dielectric constant and capacitance can be described by [43].

$$\frac{C_{ph}}{C_d} = \left(\frac{\varepsilon_{ph}}{\varepsilon_d}\right)^n, \tag{12}$$

The factor n is related to dielectric (morphology). So, Eq. (11) can be modified as:

$$\frac{C_{ph}}{C_d} = \left(\frac{3\varepsilon_o + 2N_d\alpha_d[1 + \log(1 + kL)]}{3\varepsilon_o + 2N_d\alpha_d}\right)^n, \tag{13}$$

According to Eq. (13), the relative capacitance C_{ph}/C_d is directly proportional to the illumination intensity L. The illumination dependence of the relative capacitance C_{ph}/C_d at different frequency is shown in Fig. 5. It is clear from Fig. 5 that, the relative capacitance increases exponentially with the illumination intensity which agrees with Eq. (13). This behavior was attributed to the increase of the concentration of charge carriers at the interfacial states. Therefore, the polarizability due to the charge transfer

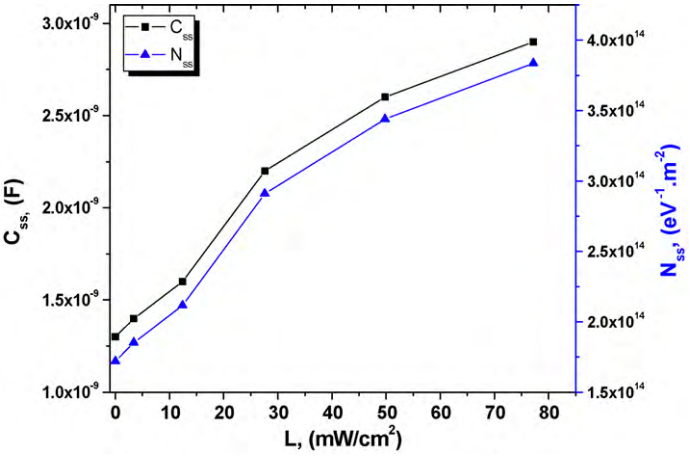

Fig. 6. Illumination dependence of both N_{ss} and C_{ss}.

of electrons and holes will be increased. In the view of the above consideration, the relative capacitance could be explained with the illumination intensities.

Capacitance spectroscopy is a widely used method which determines the variation of the interface state capacitance as a function of the forward bias at low frequency [44–46]. The capacitance of the device depending on the frequency is given as [21,44,45,47]:

$$C = C_{sc} + C_{ss} \quad \text{(at the lower frequency)}, \tag{14}$$

$$C \cong C_{sc} \quad \text{(at the higher frequency)}, \tag{15}$$

where C_{sc} is the space charge capacitance, and C_{ss} is the interface capacitance. The interface capacitance can be described as [45]:

$$C_{ss} = AqN_{ss}\frac{Arc\tan(\omega t)}{\omega\tau}, \tag{16}$$

where τ is the time constant which can be written as:

$$\tau = \frac{1}{\nu_{th}\sigma_{ss}N_{dd}}\exp\left(\frac{qV_d}{kT}\right), \tag{17}$$

where σ_{ss} is the cross-section of interface states, ν_{th} is the thermal velocity of the carrier, N_{dd} is the doping concentration, q is the electron charge and k is the Boltzmann's constant. The interface state density for small values of $\omega\tau$ is equal to [44,46,47]:

$$N_{ss} = \frac{C_{ss}}{qA}, \tag{18}$$

where A is the diode area. The interface state capacitance C_{ss} is determined from the vertical axis intercepts of C–f plots at different illuminations as shown in Fig. 2. The values of C_{ss} at different illumination intensities were used to determine the density of interface states. The distribution of the interface density states N_{ss} and the interface capacitance C_{ss} versus the illumination intensity are shown in Fig. 6. It is clear from Fig. 6 that both N_{ss} and C_{ss} increase with increasing the illumination according to different factors such as: (1) concentration of charge carriers, (2) the polarizability due to the charge transfer, (3) the interfacial polarization, and (4), the density of interface states. All of these factors affecting the increase of the interface density states as well as the interface capacitance with the illumination. The source of the interface density states N_{ss} may be due to the dangling bond at the n-GaAs surface due to the interfacial region of thickness and the native oxide that typically exists at the inorganic semiconductor surface. The tunnel-transparent oxide layer allows charge transfer between the deposited layers and the n-GaAs. The chemical interaction at the interface of the ZnTe/CdMnTe to the n-GaAs as at the other oxide–inorganic interface states will give rise to new inter-

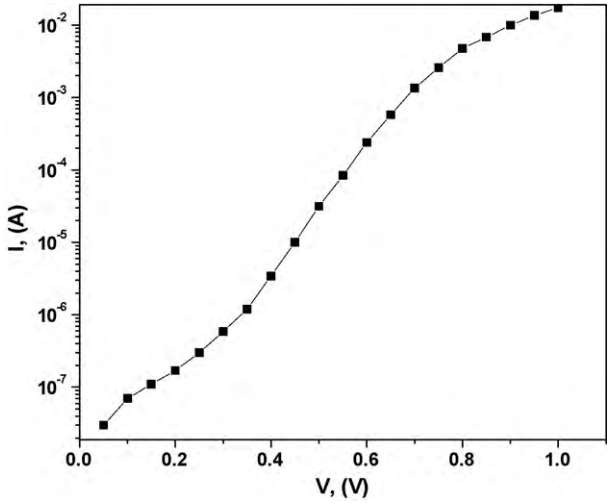

Fig. 7. Semi-logarithmic forward bias *I–V* characteristic at room temperature of the investigated device.

face states. The effect of illumination can be considered as a new source of rising the interface density states.

The *I–V* characteristics are useful to identify the carrier transport mechanisms through the junction. A semi-logarithmic forward bias *I–V* characteristic of the investigated device at room temperature is shown in Fig. 7. At the lower bias voltages ($V < 0.4$ V), the conduction mechanism can be described by the thermionic emission model. The diode current can be described as a function of applied bias voltage by [48]:

$$I = I_s \left(\exp\left(\frac{qV}{nkT} \right) - 1 \right), \tag{19}$$

where n is the ideality factor, I_s is the saturation current, T is the absolute temperature, and V is the applied voltage. The saturation current I_s is given by [49]:

$$I_s = AA^*T^2 \exp\left(-\frac{q\phi_B(IV)}{kT} \right), \tag{20}$$

where $A^* = 4\pi\, q\, m^* k^2/h^3$ is the Richardson constant which equal 8.16 A K^{-2} cm^{-2} for n-GaAs [50,51], ϕ_B is the potential barrier. The values of I_s, n and ϕ_B equal 1.581×10^{-8} A, 3.3, and 0.803 eV, respectively. The value of n not equal one, which means that the deviation from the ideal *I–V* characteristics. The higher value of n may be due to the potential drop in the interfacial layer and presence of excess current and the recombination current through the interfacial states between the semiconductor/insulator layers.

The energy of the interface states E_{ss} with respect to the bottom of conduction band at the surface of the semiconductor is described as [19,52,53]:

$$E_c - E_{ss} = q(\phi_B - V), \tag{21}$$

where E_{ss} is the energy of interface states and E_c is the bottom of the conduction band. As seen from Fig. 8 that the interface states density are decreased with the increase of $E_c - E_{ss}$. In other words, it increased with increasing the applied voltage. The exponential growth of the interface state density from midgap towards the bottom of the conduction band is very apparent. Hence, the interface state density N_{ss} values will decrease with the increase of the applied voltage. This confirms that the density of interface states changes with the biasing voltage and at each of the applied bias corresponds to a position inside the GaAs gap. The potential drop across the interfacial layer varies with the voltage bias because of the change in the charge of the interface states. So, the interface state energy distribution alerts

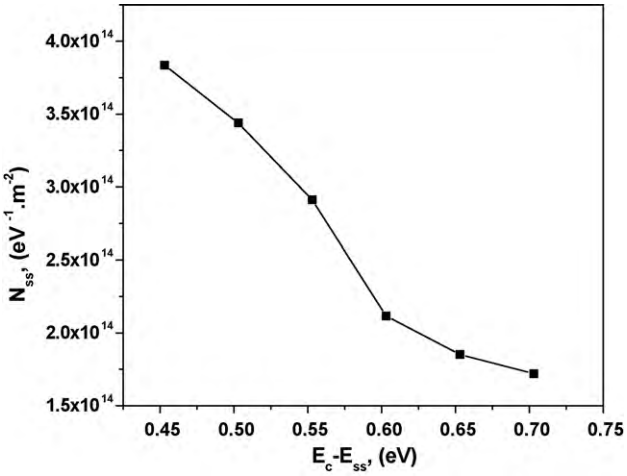

Fig. 8. The distribution plot of the interface state density N_{ss} versus $E_c - E_{ss}$.

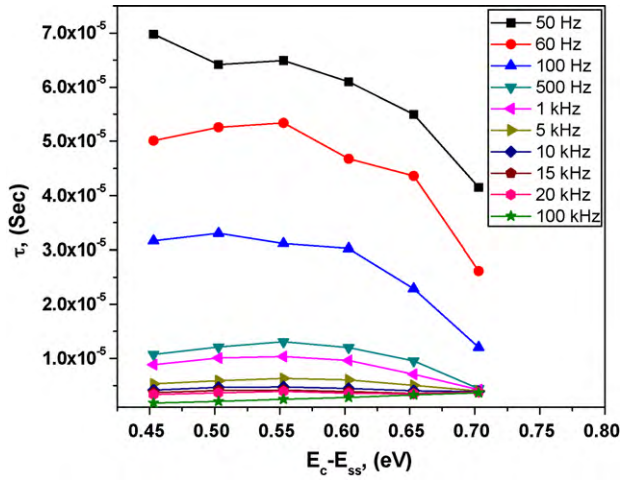

Fig. 9. Dependence of the relaxation time τ on the energy of the interface states $E_c - E_{ss}$ at different frequencies.

the diffusion potential and therefore, the depletion capacitance [44,54,55].

The dielectric relaxation time (time constant of the circuit) is used to characterize the frequency response of various signal processing systems. In *RC* circuit containing a charged capacitor and a resistor, the voltage decays exponentially as: $V(t) = V_o e^{-t/RC}$, where $RC = \tau$ is the characteristic/relaxation time of the circuit. For instance, the properties of a dielectric change on a time scale is determined by the relaxation time when an external electric field is changed. The dielectric relaxation time is a property of a solid that is closely related to its conductivity. The dielectric relaxation time is a measure of the time it takes for the charge in a semiconductor to become neutralized by conduction process. It has large values in semiconductors and insulators compared with that for metals. Dielectric relaxation as a whole is a result of the movement of dipoles (dipole relaxation) and electric charges (ionic relaxation) due to an applied alternating field. It is usually observed in the frequency range 10^2 to 10^{10} Hz [56].

The dependence of the dielectric relaxation time τ on the biasing voltages as it is converted to be a function of E_{ss} using Eq. (21) is shown in Fig. 9 at different frequencies. From Fig. 9, it is clear that the relaxation time τ decreased with increasing the energy $E_c - E_{ss}$. Also, at any value of $E_c - E_{ss}$, it decreased with increasing the frequency. Furthermore, the relaxation time showed an exponential decrease with biasing voltage

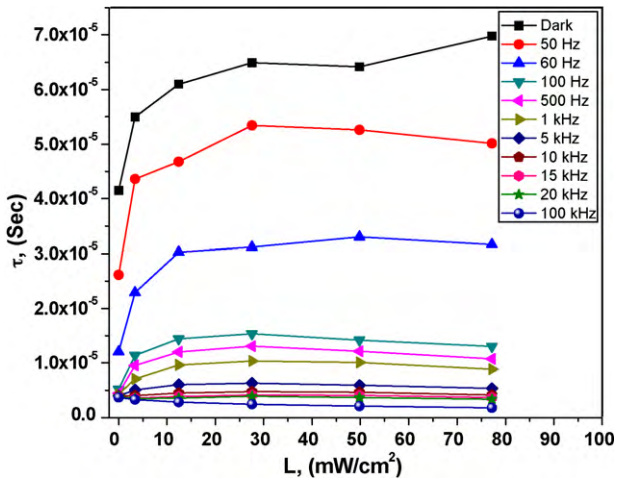

Fig. 10. Illumination dependence of the relaxation time τ at different frequencies.

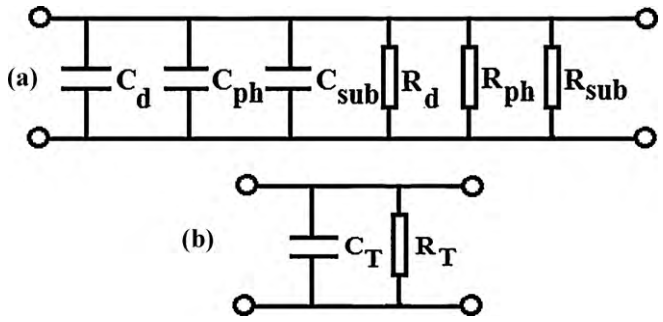

Fig. 11. (a) Simplified circuit. (b) Equivalent circuit of the p-ZnTe/n-CdMnTe/GaAs.

with respect to the bottom of the conduction band towards the midgap. Thus, it can be said that the relaxation time to be bias-dependent.

Dependence of the relaxation time τ on the illumination at different frequencies is shown in Fig. 10. It is clear from Fig. 10 that the relaxation time increased with increasing the illumination intensities while it decreased with increasing the applied frequencies. The increase of the interfacial capacitance with illumination may be due to multicomponent of polarization such as: dipolar, ionic polarization, electronic and interfacial polarization. Accordingly, the increase of the relaxation time with the increase of the capacitance under the effect of light could be explained. It is generally known that, the relation between the relaxation time τ, the relative dielectric constant ε_r and the conductivity σ are given by: $\tau = \varepsilon_r \varepsilon_o / \sigma$ [56]. Besides, the relative dielectric constant ε_r decreases with increasing the applied frequency. So, the decrease of relaxation time with increasing the applied field is expected.

Therefore, it is concluded that the interface capacitance C, the cell resistance R and hence the relaxation time τ should decrease with increasing the frequency. Such behavior of C, R and τ can be explained on the basis of assumption that only almost all of the interface states cannot follow the applied ac signal sufficiently at the higher frequency [57].

Simplified and equivalent circuits of the prepared p-ZnTe/n-CdMnTe/GaAs magnetic heterostructure device for photocapacitance applications are shown in Fig. 11. Circuit contains actually three basic capacitances due to three kinds of dielectric: ZnTe/CdMnTe (dark C_d and illumination C_{ph}) and GaAs substrate (C_{sub}). There are three kind of resistance associated with the three capacitance in parallel connection: ZnTe/CdMnTe (dark R_d and illumination R_{ph}) and GaAs substrate (R_{sub}). The equivalent circuit reflects the point between the photocapacitance and the photoconductivity of p-ZnTe/n-CdMnTe/GaAs which have a common physical interpretation as photo-generation of electrons/holes under the effect of illumination [23].

4. Conclusions

Heterostructure of p-ZnTe/n-CdMnTe/GaAs was grown by MBE technique. The prepared device showed a light sensitive capacitor. The capacitance and the resistance of the prepared device showed an illumination dependence. The increase of the capacitance with illumination is associated with polarization due to the transfer of photo-generated electrons and holes. But, the decrease of resistance with illumination is associated with the generation of charge carriers. The increase of N_{ss}, C_{ss}, C_{ph}/C_d and τ with illumination were attributed to the multicomponent of polarization such as: dipolar, electronic, ionic and interfacial polarization. The frequency and illumination dependence of the interfacial capacitance can be interpreted according to the modified Goswami and Goswami (G–G) model. The effect of illumination was considered as a new source of rising the interface density states. Finally, p-ZnTe/n-CdMnTe/GaAs can be a good candidate material in a light sensitive capacitor in modern electronic devices.

Acknowledgments

One of the authors (I.S. Yahia) would like to acknowledge the partnership and ownership initiative (PAROWN) of Egyptian Ministry of Higher Education and State for Scientific Research. Especial thanks to Prof. Dr. G. Karczewski, Institute of Physics, Polish Academy of Sciences, Warszawa, Poland for the preparation of the studied sample.

References

[1] S.P. Nehra, M. Singh, J. Alloys Compd. 488 (2009) 356–359.
[2] A.M. Abdel Hakeem, J. Magn. Magn. Mater. 322 (2010) 709–714.
[3] A. Alsaad, Physica B 405 (2010) 951–954.
[4] S.A. Touat, F. Litimein, A. Tadjer, B. Bouhafs, Physica B 405 (2010) 625–631.
[5] L.-C. Tung, G. Karczewski, Y.J. Wang, Physica E 40 (2008) 1608.
[6] P. Banerjee, B. Ghosh, J. Alloys Compd. 484 (2009) 712–717.
[7] J.K. Furdyna, J. Kossut, Semiconductors and Semimetals, vol. 25: Diluted Magnetic Semiconductors, Boston, Academic, 1988;
J.K. Furdyna, J. Kossut, Semiconductors and Semimetals, vol. 25: Diluted Magnetic Semiconductors, Mir, Moscow, 1992.
[8] W.H. Ko, Q. Wang, Sens. Actuators A-Phys. 75 (1999) 242.
[9] A.A. Ned, R.S. Okojie, A.D. Kurtz, Proc. High Temp. Electronics Conf, IEEE, Piscataway, NJ, 1998.
[10] C.H. Wu, S. Stefanescu, H.I. Kuo, C.A. Zorman, M. Mehregany, Proc. Int. Conf. Solid-State Sensors and Actuators, Copenhagen, Denmark, 1997.
[11] D.J. Young, J. Du, C.A. Zorman, W.H. Ko, IEEE Sens. J. 4 (2004) 464.
[12] P. Chattopadhyay, B. RayChaudhuri, Solid-State Electron. 36 (1993) 605.
[13] J.H. Werner, K. Ploog, H.J. Queisser, Phys. Rev. Lett. 57 (1986) 1080.
[14] B. Akal, Z. Benamara, B. Gruzza, L. Bideux, Vacuum 57 (2000) 219.
[15] A. Singh, Solid-State Electron. 28 (1985) 223.
[16] S. Kochowski, B. Paszkiewicz, R. Paszkiewicz, Vacuum 57 (2000) 157.
[17] J. Fernandez, P. Godignon, S. Berberich, J. Rebollo, G. Brezenanu, J. Millan, Solid-State Electron. 39 (1996) 1359.
[18] T. Tagmouti, A. Outzourhit, A. Oueriagli, M. Khaidar, M. Elyacoubi, R. Evrard, Thin Solid Films 379 (2000) 272.
[19] B. Batı, C. Nuhoğlu, M. Sağlam, E. Ayyıldız, A. Türüt, Phys. Scr. 61 (2000) 209.
[20] M. Zamora, G.K. Reeves, G. Gazeckia, J. Mi, C.Y. Yang, Solid-State Electron. 43 (1999) 801.
[21] Ş. Aydoğan, M. Sağlam, A. Türüt, Polymer 46 (2005) 6148.
[22] A. Ashery, A.A.M. Farag, M.A. Salem, Microelectron. Eng. 85 (2008) 2309–2315.
[23] M.H. Sayyed, M. Shah, K.S. Karimov, Z. Ahmad, M. Saleem, M. Maroof Tahir, J. Optoelectron. Adv. Mater. 10 (2008) 2805.
[24] V. Dyakonov, D. Godovsky, J. Meyer, J. Parisi, C.J. Brabec, N.S. Sariciftci, J.C. Hummelen, Synth. Met. 124 (2001) 103.
[25] A. Jasenek, U. Rau, J. Appl. Phys. 90 (2001) 650.
[26] A. Jasenek, H.W. Schock, J.H. Werner, U. Rau, Appl. Phys. Lett. 79 (2001) 2922.
[27] A. Jasenek, U. Rau, K. Weinert, H.W. Schock, J.H. Werner, Appl. Phys. Lett. 82 (2003) 1410.
[28] A.E. Bekheet, Physica B 403 (2008) 4342.
[29] A. Goswami, A.P. Goswami, Thin Solid Films 16 (1973) 175.

[30] H.S. Nalwa, P. Vasudevan, J. Mater. Sci. Lett. 2 (1983) 71.
[31] R.D. Gould, A.K. Hassan, Thin Solid Films 223 (1993) 334.
[32] T.D. Anthopoulos, T.S. Shafai, J. Appl. Phys. 94 (2003) 2426.
[33] M.A.M. Seyam, Appl. Surf. Sci. 181 (2001) 128.
[34] P.W. Zukowski, S.B. Kantorow, D. Maczka, V.F. Stelmakh, Phys. Status Solidi (a) 112 (1989) 695.
[35] A. Vasudevan, S. Carin, M.R. Melloch, E.S. Harmon, Appl. Phys. Lett. 73 (1998) 671.
[36] A.M.A. El-Barry, H.E. Atyia, Physica B 368 (2005) 1.
[37] F. Gutman, L.E. Lyons, Organic Semiconductors, Robert E. Krieger Publishing Company, Malabar, FL, 1980.
[38] A.Y.C. Chan, Electron. Lett. 22 (1986) 11.
[39] M. Ali Omar, Elementary Solid State Physics: Principles and Applications, Pearson Education Pte. Ltd., Singapore, 2002.
[40] V.A. Kargin (Ed.), Organic Semiconductors, Nauka, Moscow, 1968.
[41] M. Iwamoto, T. Manaka, Proc. Int. Symp. Super—Functionality Organic Devices, IPAP Conf. Series 6, 2005.
[42] F. Amy, C. Chan, A. Kahn, Org. Electron. 6 (2005) 85.
[43] Z.M. Rittersma, Sens. Actuators A-Phys. 96 (2002) 196.
[44] A. Türüt, M. Sağlam, Physica B 179 (1992) 285.
[45] E.H. Nicollian, A. Goetzberger, Bell Syst. Technol. 46 (1967) 1055.
[46] F. Chekir, C. Baret, A. Vapaille, J. Appl. Phys. 54 (1983) 6474.
[47] P. Cova, A. Singh, R.A. Masut, J. Appl. Phys. 82 (1997) 217.
[48] S.M. Sze, Physics of Semiconductor Devices, Physics and Technology, second ed., Wiley, New York, 2001.
[49] Ö. Vural a, Y. Şafak b, Ş. Altindal b, A. Türüt, Curr. Appl. Phys. 10 (2010) 761.
[50] M. Daraee, M. Hajian, M. Rastgoo, L. Lavasanpour, Adv. Stud. Theor. Phys. 2 (2008) 957–964.
[51] A.F. Özdemir, A. Türüt, A. Kökce, Thin Solid Films 425 (2003) 210.
[52] B. Akal, Z. Benamara, L. Bideux, B. Gruzza, Microelectron. J. 30 (1999) 637.
[53] P. Cova, A. Singh, Solid-State Electron. 33 (1990) 11.
[54] S.M. Sze, Physics of Semiconductor Devices, second ed., Wiley, New York, 1981.
[55] E.H. Rhoderick, Metal–Semiconductor Contacts, Oxford University Press, Oxford, 1978.
[56] P. Lorrain, D.R. Corson, F. Lorrain, Electromagnetic Fields and Waves (Including Electric Circuits), third ed., W.H. Freeman and Company, New York, 1996.
[57] R. Şahingöza, H. Kanbur, M. Voigt, C. Soykan, Synth. Met. 158 (2008) 727–731.